JOURNAL OF Materials CHEMISTRY

Chemistry of interstitial molybdenum ternary nitrides M_nMo_3N (M = Fe, Co, $n = 3$; M = Ni, $n = 2$)

Silvia Alconchel,‡ Fernando Sapiña,*† Daniel Beltrán and Aurelio Beltrán

Institut de Ciència dels Materials de la Universitat de València, C/Doctor Moliner 50, 46100 Burjassot, Spain

Interstitial molybdenum ternary nitrides, M_nMo_3N (M = Fe and Co, $n = 3$; M = Ni, $n = 2$), can be obtained by ammonolysis of molybdate precursors, $MMoO_4 \cdot nH_2O$. A study of the influence of the preparative variables on the outcomes from this procedure is presented. Fe_3Mo_3N and Co_3Mo_3N are prepared as nearly single phases at temperatures as low as 973 K, but higher temperatures are required to obtain pure samples (1073 and 1173 K for Fe and Co compounds, respectively). In the case of Fe_3Mo_3N, moreover, a slow cooling of the samples results in segregation of impurities. The nickel nitride derivative shows a different stoichiometry, Ni_2Mo_3N, which results in the systematic presence of impurities. The structures of M_3Mo_3N (M = Fe, Co) have been refined from X-ray powder diffraction data. These nitrides crystallize in the cubic system, space group $Fd\bar{3}m$ [$a = 11.076\,33(8)$ and $11.023\,96(8)$ Å for M = Fe and Co, respectively]. The structure of Ni_2Mo_3N has been determined in an *ab initio* manner from X-ray powder diffraction data. The cell is cubic, space group $P4_132$ [$a = 6.634\,22(4)$ Å]. Starting positional parameters were obtained by direct methods, and the structure was refined by Rietveld analysis of the data. All three nitrides are prepared as phases constituted by submicrometer homogeneous particles. They show metallic behavior, and temperature programmed oxidation studies reveal an enhanced stability for the nickel derivative in an oxygen atmosphere.

Introduction

The traditional interest in transition-metal carbides and nitrides is currently growing as more applications for these materials arise.[1] Indeed, besides classical uses, such as those related to their strength and durability exploited in industrial tools,[2] the chemical and structural versatility of these materials, and other related ones, is resulting in the discovery of many new phases with relevant optical, electrical and magnetic properties suitable for technical developments, without prejudice to their basic interest.[3] Thus, for example, superconductivity has been recently reported in alkali-metal halogenonitrides, A_xZrNCl,[4] and in fields such as catalysis, nitrides as well as carbides are attracting considerable attention because of their exceptional reactivity, which is also leading to emerging applications.[5]

Molybdenum nitrides constitute examples of promising catalytic materials: they have proved to be active and selective in processes involving hydrogen transfer reactions, such as hydrodenitrogenation (HDN) and hydrodesulfurization (HDS).[6] Recently, it has been also shown that the catalytic activity of molybdenum nitrides is enhanced by addition of another transition metal such as vanadium.[7] In fact, the V–Mo oxynitride presents higher activity in quinoline hydrodenitrogenation than vanadium or molybdenum nitrides alone.

From the above, it seems reasonable to view transition metal–molybdenum ternary nitrides as suitable materials to be studied owing to their potential catalytic activity. Until now, several transition metal–molybdenum ternary nitrides have been claimed to be prepared, namely $MnMoN_2$,[8] $(Fe_{0.8}Mo_{0.2})MoN_2$ [9] and M_3Mo_3N (M = Fe, Co, Ni).[10,11] Whilst the two first compounds are described as covalent ternary molybdenum nitrides, nitrogen in M_3Mo_3N derivatives should have interstitial character.

The ternary interstitial nitrides, M_3Mo_3N (M = Fe, Co), were first synthesized by Bem *et al.* by ammonolysis of oxide precursors, and reported to be isostructural to η-Fe_3W_3C.[10,11] Fe_3Mo_3N has been also prepared by heating alkanolamine complexed precursors in ammonia[12] or by reaction between Fe–Mo particles and gaseous N_2 or NH_3.[13] Concerning 'Ni_3Mo_3N', the results described in the literature are, however, controversial. Bem *et al.*[11] synthesized this nitride by ammonolysis of an oxide precursor, and the diffractogram of the resulting product was indexed to an orthorhombic unit cell. However, Weil and Kumta,[12] who also prepared 'Ni_3Mo_3N' in the same way but under different synthetic conditions, presented an X-ray diffraction pattern of their product clearly different from that reported by Bem *et al.*[11]

It seems evident that, in dealing with complex systems such as those above, a careful control of the procedural variables is required in order to obtain well characterized ternary derivatives: even more so if the ultimate aim is a rational design of catalyst materials, which should not be guided only by trial and error assays. In the present work we report the study of the influence of synthetic variables in the preparation of interstitial molybdenum ternary nitrides by ammonolysis of oxide precursors. As well as establishing the optimal conditions for the preparation of pure samples of M_3Mo_3N (M = Fe, Co), their structures have been refined from X-ray powder diffraction data. The analogous nickel derivative shows different stoichiometry, Ni_2Mo_3N, and its structure has been determined in an *ab initio* manner from X-ray powder diffraction data. Temperature programmed oxidation experiments allow us to advance preliminary conclusions regarding the stability of these nitrides under oxidative conditions.

Experimental

Synthesis

Materials used in this work were $FeCl_2 \cdot 4H_2O$ (Merck, 99%), $CoCl_2 \cdot 6H_2O$ (Panreac, 99%), $NiCl_2 \cdot 6H_2O$ (Panreac, 97%) and $Na_2MoO_4 \cdot 2H_2O$ (Panreac, 98%).

Molybdate precursors were prepared by dropwise addition of 250 ml of an aqueous solution (0.25 M) of the appropriate metal chloride to an equal volume (250 ml) of an equimolar solution (0.25 M) of sodium molybdate. The precipitates

†E-mail: fernando.sapina@uv.es
‡Permanent address: Departamento de Química General e Inorgánica, Facultad de Ingeniería Química, Universidad Nacional del Litoral, Santiago del Estero 2829, 3000 Santa Fe, Argentina.

formed were refluxed in the mother-liquor for 24 h to improve their crystallinity. Then, the solids were filtered off, washed with distilled water and dried at 393 K for 24 h. The products were a brown powder (FeMoO precursor), a violet powder (CoMoO precursor) and a green powder (NiMoO precursor).

Ternary nitrides were synthesized by ammonolysis of the molybdate precursors. The gases employed were NH_3 (99.9%) and N_2 (99.9995%). A sample of the selected precursor (0.5 g) was placed into an alumina boat, which was then inserted into a quartz flow-through tube furnace. The back end of the tube furnace was connected to an acetic acid trap and the front end was connected to the gas line or to a vacuum pump. Prior to initiating the thermal treatment, the tube furnace was evacuated under vacuum for 20 min, then purged for 10 min with N_2 and another 20 min with NH_3. Several runs under different experimental conditions were also performed in order to determine the appropriate conditions for the preparation of each of the nitrides. The precursor powder was heated at 5 K min^{-1} to a final temperature (T_f) that was held for a period of time (t_{hold}) under flowing ammonia (50 cm^3 min^{-1}). Then, the solid was cooled down at variable rates (r_c) in the same atmosphere. The different cooling rates were obtained by either turning off the oven and leaving the sample inside (slow, *ca.* 2 K min^{-1}) or by quenching at room temperature (fast, *ca.* 50 K min^{-1}). After cooling, the product was purged with N_2 for 10 min. Some samples tend to be pyrophoric, and were 'passivated' for 20 h in an N_2 flow (50 cm^3 min^{-1}) at room temperature. All products were stored in a desiccator over $CaCl_2$. The main synthetic variables are summarized in Table 1.

For resistivity measurements, nitride sample powders were pressed at 15 MPa for 3 min and formed into discs of 12 mm diameter and thickness 0.8–1.0 mm. These pellets were sintered under flowing ammonia (50 cm^3 min^{-1}) for 6 h under the same conditions as those used to prepare the starting powders.

Characterization

Elemental analysis. Metal ratios in the solids were determined by energy dispersive X-ray analysis (EDAX) on a JEOL JSM 6300 scanning electron microscope collected by a Oxford detector with quantification performed using virtual standards on associated Link-Isis software. The operating voltage was 20 kV, and the energy range for analysis 0–20 keV. Quantitative chemical analyses of metals were also carried out by inductively coupled plasma–mass spectroscopy (ICP–MS) with a Jobin-Yvon JY24 spectrophotometer. A small amount of each powder (20 mg) was dissolved in concentrated HNO_3 and diluted to 100 ml with distilled water.

Thermogravimetric measurements, performed with a Perkin Elmer TGA 7 system, were used to determine the water content of the precursors by heating the samples under Ar at 5 K min^{-1} to 973 K (FeMoO precursor) or 1173 K (CoMoO and NiMoO precursors).

The nitrogen content of the nitrides was evaluated by standard combustion analysis (Carlo Erba EA 1108). The oxygen impurity content of nitrides was also indirectly determined by heating in air the nitrides (TGA experiments) to 973 K for the Fe sample and 1173 K for the Co and Ni samples, and comparing the observed weight increase with the combustion analysis results.

Tables 2 and 3 summarize the results of these analyses for both the molybdate precursors and the resulting nitrides, respectively. As can be observed, the total M/Mo ratio is, in all cases, equal to unity (within experimental error).

X-Ray diffraction. X-Ray powder diffraction patterns were obtained from a Seifert C-3000 θ–θ automated diffractometer using graphite-monochromated Cu-Kα radiation. Powder samples were mixed with acetone to form a slurry and mounted on a glass slide. Routine patterns for phase identification were collected with a scanning step of 0.08° in 2θ over the angular range 10–70° in 2θ with a collection time of 3 s $step^{-1}$. For Rietveld analysis, patterns were collected with a scanning step of 0.02° in 2θ, over a wider angular range (2θ 20–140°), and with a longer acquisition time (10 s $step^{-1}$) in order to enhance statistics. The TREOR program was used to index the patterns.[14,15] Rietveld analyses were performed with the FULLPROF program.[16] The fits were performed using a pseudo-Voigt peak-shape function. In the final runs, usual profile parameters (scale factors, background coefficients, zero-points, half-width, pseudo-Voigt and asymmetry parameters for the peak-shape) and atomic positions were refined. Isotropic thermal parameters were set at 0.3 and 0.7 $Å^2$ for metal and nitrogen atoms, respectively, and an overall thermal parameter was also refined. Residuals given in Tables 4 and 5 are the conventional (background corrected) peak only Rietveld profile and weighted profiles residuals, R_p and R_{wp}, and the integrated intensity and structure factor residuals, R_B and R_F.

Table 1 Experimental preparation conditions of transition metal nitrides, M_nMo_3N (M = Fe, Co, n = 3; M = Ni, n = 2)[a]

sample	final temperature/ K	time hold/ h	cooling[b]	passivation[c]
FeMoN-A	873	12	fast	yes
FeMoN-B	973	12	fast	yes
FeMoN-C	1073	12	fast	yes
FeMoN-D	1073	12	slow	yes
FeMoN-E	1073	2	fast	yes
FeMoN-F	1173	12	fast	no
CoMoN-A	873	12	fast	yes
CoMoN-B	973	12	fast	no
CoMoN-C	1073	12	fast	no
CoMoN-D	1173	12	fast	no
CoMoN-E	1173	12	slow	no
CoMoN-F	1173	2	fast	no
NiMoN-A	873	12	slow	no
NiMoN-B	973	12	slow	no
NiMoN-C	1073	12	slow	no
NiMoN-D	1073	2	slow	no
NiMoN-E	1223	4	slow	no
NiMoN-F	1223	4	fast	no

[a]Heating rate: 5 K min^{-1}; ammonia flow rate: 50 cm^3 min^{-1}. [b]fast ≈ 50 K min^{-1} ; slow ≈ 2 K min^{-1}. [c]Under flowing N_2 (50 cm^3 min^{-1}, O_2 ≤ 1 ppm) at room temperature for 20 h.

Table 2 Chemical composition of mixed-metal molybdate precursors

sample	M(atom%)/ Mo(atom%)[a]	weight loss[b] (%)	water content[c], x
FeMoO	1.06 (1.05)	6.82 (863 K)	0.88
CoMoO	0.88 (0.91)	7.55 (773 K)	0.97
NiMoO	0.95 (0.95)	8.45 (773 K)	1.11

[a]ICP-MS (EDAX). [b]TGA. [c]Calculated for $MMoO_4$ (M = Fe, Co, Ni) final composition.

Table 3 Chemical composition of selected powder nitrides

sample	M(atom%)/ Mo(atom%)[a]	Nitrogen (wt.%)[b]
FeMoN-C	0.97 (1.09)	2.84 (2.98)[c]
FeMoN-E		2.89
FeMoN-F		3.21
CoMoN-D	0.89 (1.07)	2.96 (2.93)
CoMoN-E		2.65
CoMoN-F		2.68
NiMoN-C	0.95 (0.95)	3.30
NiMoN-D		3.08

[a]ICP-MS (EDAX). [b]C, H and N combustion analysis. [c]Value for M_3Mo_3N composition (M = Fe, Co).

Table 4 Structural data from X-ray powder diffraction studies of M_3Mo_3N (M = Fe, Co)

atom	Wyckoff	x	y	z
		Fe_3Mo_3N		
		space group, $Fd\bar{3}m$, $a = 11.076\ 33(8)$ Å		
Fe(1)	32e	0.29382(8)	0.29382(8)	0.29382(8)
Fe(2)	16d	1/2	1/2	1/2
Mo	48f	0.32159(6)	1/8	1/8
N	16c	0	0	0
		$R_p = 11.1$, $R_{wp} = 14.9$, $R_B = 3.24$, $R_F = 2.46$[a]		
		Co_3Mo_3N		
		space group, $Fd\bar{3}\,m$, $a = 11.023\ 96(8)$ Å		
Co(1)	32e	0.29216(7)	0.29216(7)	0.29216(7)
Co(2)	16d	1/2	1/2	1/2
Mo	48f	0.32411(6)	1/8	1/8
N	16c	0	0	0
		$R_p = 10.1$, $R_{wp} = 13.7$, $R_B = 2.78$, $R_F = 2.44$		

[a]The observed intensitities have been corrected for background; only points where there are Bragg contributions have been included in the calculation of R_p and R_{wp}. $R_p = \Sigma |y_i(\text{obs}) - y_i(\text{calc})| / \Sigma y_i(\text{obs})$, $R_{wp} = \{\Sigma w_i[y_i(\text{obs}) - y_i(\text{calc})]^2 / \Sigma w_i[y_i(\text{obs})]^2\}^{1/2}$, $R_B = \Sigma |I_K(\text{'obs'}) - I_K(\text{calc})| / \Sigma I_K(\text{'obs'})$ $R_F = \Sigma |I_K(\text{'obs'})^{1/2} - I_K(\text{calc})^{1/2}| / \Sigma I_K(\text{'obs'})^{1/2}$.

Microstructural characterization. The morphology of both the molybdate precursors and the nitrides was observed using a scanning electron microscope (Hitachi S-4100) operating at an accelerating voltage of 30 kV. The powders were dispersed in ethanol and treated with ultrasound for 10 min. All the samples were covered by a thin film of gold for better image definition.

Oxidation behavior. In addition to thermogravimetric measurements, temperature-programmed oxidation of the nitrides was carried out using a Micromeritics TPD/TPR 2900 instrument equipped with a thermal conductivity detector. In a typical TPO experiment, 50 mg of the powder were contacted with the reactant 2% (v/v) O_2–He flow (50 cm^3 min^{-1}), while the temperature was raised at 5 K min^{-1}.

Resistivity measurements. Dc resistivity measurements were performed on sintered pellets with a standard four-probe technique. Measurements in the temperature range 30–300 K were performed in a He closed-cycle Leybold–Heraeus cryostat. The samples had approximately the same dimensions (typically $1.0 \times 3.00 \times 4.00$ mm).

Results and Discussion

Synthesis

X-Ray powder diffraction patterns show that all the precursor molybdates are crystalline. Co and Ni precursor patterns correspond to JCPDS card 14,0086 ($CoMoO_4 \cdot 0.9H_2O$) and JCPDS card 13,0128 ($NiMoO_4 \cdot xH_2O$), whereas the Fe precursor pattern cannot be identified from this database. SEM scanning images (see below) show that the precursors are formed by elongated crystals with typical dimensions around $1500 \times 150 \times 150$ nm for the Fe and Co precursors, and $800 \times 100 \times 100$ nm for the Ni precursor.

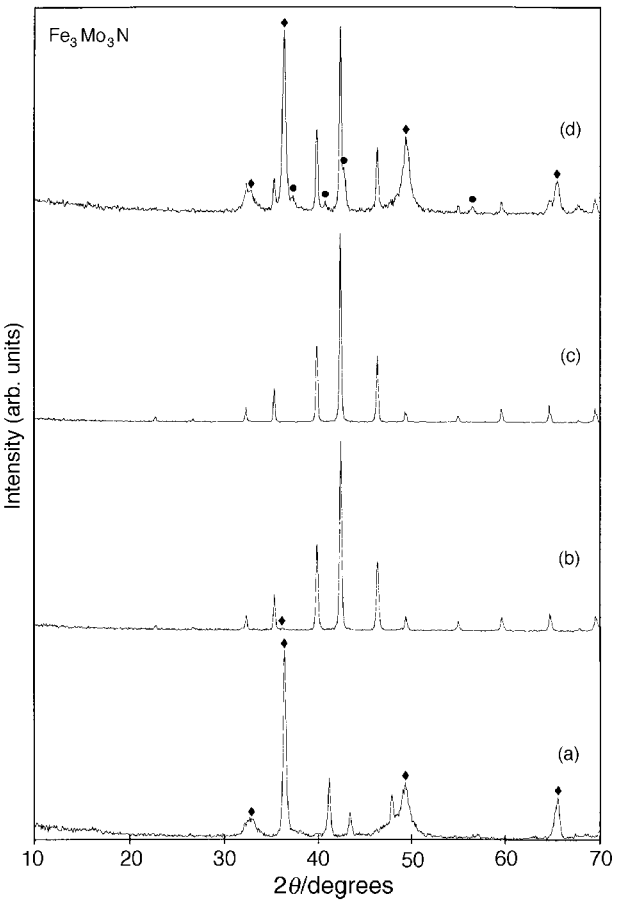

Fig. 1 X-Ray diffraction patterns of the products resulting after ammonolysis of the FeMoO precursor under different synthetic conditions: a) $T_f = 873$ K, fast cooling (sample FeMoN-A), b) $T_f = 973$ K, fast cooling (sample FeMoN-B), c) $T_f = 1073$ K, fast cooling (sample FeMoN-C/E) and d) $T_f = 1073$ K, slow cooling (sample FeMoN-D). Reflections marked with ◆ and ● are those identified as corresponding to $(Fe_{0.8}Mo_{0.2})MoN_2$ and Fe_2N (JCPDS card 06,0656).

Fig. 1–3 show the X-ray powder diffraction patterns of the products that result from the ammonolysis of the precursors using different synthetic variables. From these experiments, it can be first noted that the minimum temperature at which the nitrides can be obtained as majority phases is 973 K for the Fe and Co compounds, and 1073 K for the Ni compound.

Dealing with the Fe compound (Fig. 1), it is noteworthy that, besides temperature, the cooling rate also plays a significant role for obtaining the pure nitride. Thus, although 973 K is the temperature at which the compound already appears as the majority phase (in fact, as a nearly single phase), impurity peaks of low intensity can be observed [Fig. 1(b)]. These impurity peaks are absent in the pattern of the sample prepared at 1073 K when it is rapidly cooled [Fig. 1(c)]. However, slow cooling of samples prepared at 1073 K [Fig. 1(d)] or treatment

Table 5 Structural data from X-ray powder diffraction studies of Ni_2Mo_3N

atom	Wyckoff	x	y	z	fraction
		Ni_2Mo_3N			
		space group, $P4_132$, $a = 6.634\ 22(4)$ Å			
Ni(1)	8c	0.18354(16)	0.18354(16)	0.18354(16)	1.0
Mo	12d	0.79857(8)	0.04857(8)	1/8	0.986(8)
Ni(2)	12d	0.79857(8)	0.04857(8)	1/8	0.014(8)
N	4b	7/8	7/8	7/8	1.0
		$R_p = 10.2$, $R_{wp} = 12.9$, $R_B = 2.88$, $R_F = 2.21$.			

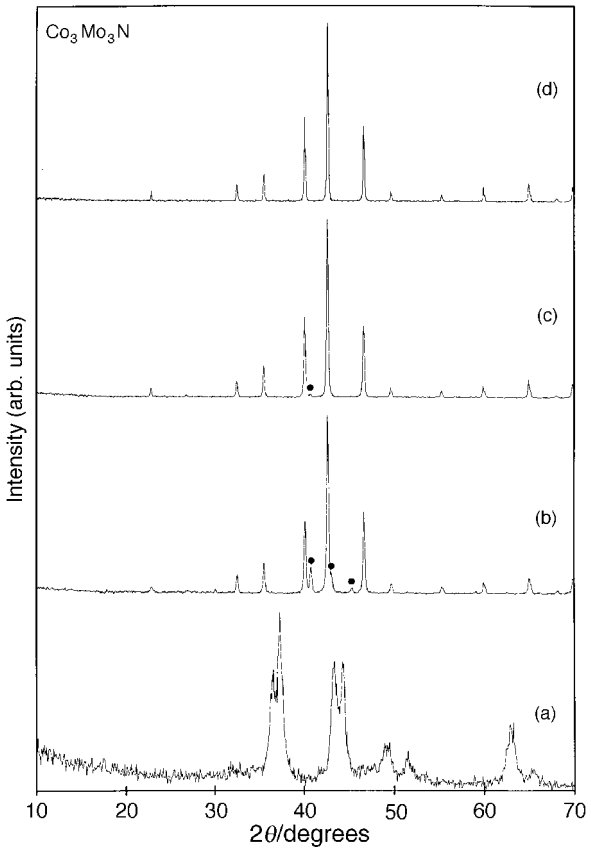

Fig. 2 X-Ray diffraction patterns of the products resulting after ammonolysis of the CoMoO precursor under different synthetic conditions: a) $T_f = 873$ K (sample CoMoN-A), b) $T_f = 973$ K (sample CoMoN-B), c) $T_f = 1073$ K (sample CoMoN-C) and d) $T_f = 1173$ K (sample CoMoN-D/E/F). Reflections marked with ● are those identified as corresponding to the more intense reflections in the pattern of the Ni compound.

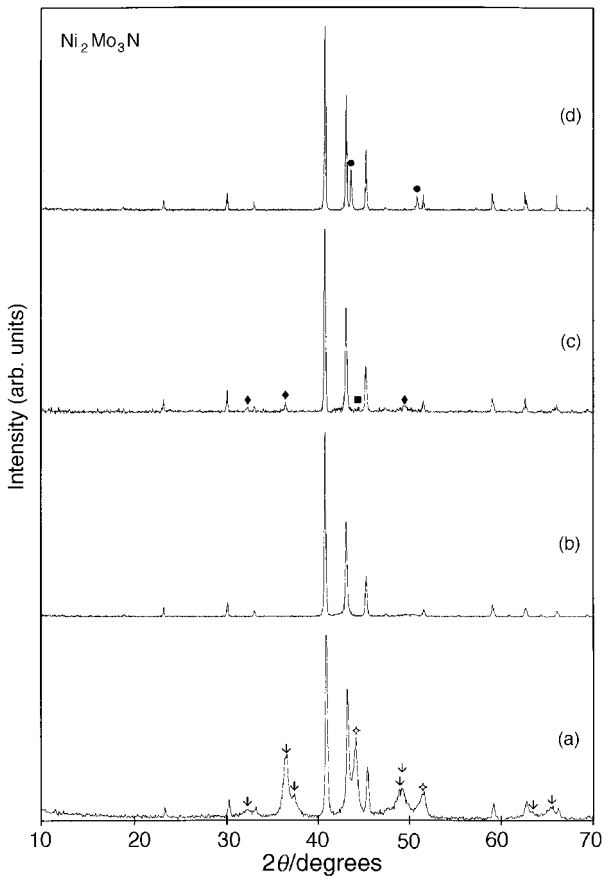

Fig. 3 X-Ray diffraction patterns of the products resulting after ammonolysis of the NiMoO precursor under different synthetic conditions: a) $T_f = 873$ K, slow cooling (sample NiMoN-A), b) $T_f = 1073$ K, slow cooling (sample NiMoN-C/D), c) $T_f = 1223$ K, slow cooling (NiMoN-E) and d) $T_f = 1223$ K, fast cooling (sample NiMoN-F). Reflections marked with ● are those identified as corresponding to the cubic impurity; those marked with ◇ correspond to Ni_3N (JCPDS card 10,0280), and those with ↓ to molybdenum nitrides (Mo_2N and MoN; JCPDS cards 25,1366 and 25,1367) and $Ni_{0.2}Mo_{0.8}N$ (JCPDS card 29,0931).

of the precursor at lower temperatures [Fig. 1(a)] result in the presence of impurities. This behavior could be attributted to the capability of this system to absorb more nitrogen at low temperatures, thus leading to products with a lower total-metal/nitrogen ratio. In fact, Bem *et al.*[9] have prepared the compound $Fe_{0.8}Mo_{0.2}MoN_2$ by ammonolysis of $Fe_2(MoO_4)_3$ at low temperatures. Some of the impurity peaks observed in the patterns of samples obtained after slow cooling or at low temperatures are coincident with this compound and can be attributed to $Fe_{0.8}Mo_{0.2}MoN_2$. In addition, for samples prepared at high temperatures with slow cooling rates, the presence of Fe_2N (JCPDS card 06,0656) is also detected.

In contrast to the Fe compound, the cooling rate apparently plays no role in the synthesis of the Co material [Fig. 2(d)]. Notwithstanding, it must be stressed that, as can be observed by comparison of the respective patterns [Fig. 1(c) and 2(d)], both nitrides are isostructural. The intensity of the impurity peaks detectable in the pattern of the sample obtained at 973 K [Fig. 2(b)] clearly decreases in comparison to that corresponding to the 1073 K sample [Fig. 2(c)] and the Co nitride is obtained as a single phase at 1173 K [Fig. 2(d)]. Whereas it has not been possible to identify the phases present in samples prepared at low temperatures [Fig. 2(a)], it should be noted that the impurity peaks present in the 973 K sample pattern appear at practically the same 2θ values as those corresponding to the more intense reflections in the pattern of the Ni compound.

For the Ni compound (Fig. 3) different behavior from both the Fe and Co compounds is seen. In fact, while a nearly single phase is obtained at 1073 K [Fig. 3(b)] except for minor impurities, the diffraction pattern can be indexed with a primitive cubic cell (see below), impurity peaks are detected for all temperatures and cooling rates studied in this work. Moreover, the nature of the impurities (as reflected in the patterns) depends on the cooling rate. Indeed, the patterns corresponding to samples obtained at 1223 K and different cooling rates [Fig. 3(c), (d)] show, besides the reflections appearing in the 1073 K sample pattern, impurity peaks from different origins. The pattern in Fig. 3(c) (slow cooling rate, broad impurity peaks) fits in well with that reported by Weil and Kumta.[12] Although these authors directly attributted this pattern to an hypothetical 'Ni_3Mo_3N' nitride, the fact is that the additional broad impurity peaks can be identified as corresponding to Ni_3N (JCPDS card 10,0280) and $Ni_{0.2}Mo_{0.8}N$ (JCPDS card 29,0931). On the other hand, the pattern of Fig. 3(d) (fast cooling rate, sharp impurity peaks) corresponds to that reported by Bem *et al.*[11] (clearly distinguishable from the above and also assigned to a 'Ni_3Mo_3N' nitride). Although in this case the impurity peaks are not clearly identified on the JCPDS database, they can be indexed with a cubic unit cell, with a cell parameter of 3.590 Å. As we will show below, the true stoichiometry of the nickel and molybdenum nitride majority phase is Ni_2Mo_3N (in contrast to that observed for both the Fe and Co derivatives). With respect to the low temperature pattern [Fig. 3(a)] γ-Mo_2N (JCPDS card 25,1366), MoN (JCPDS card 25,1367) and $Ni_{0.2}Mo_{0.8}N$ (JCPDS card 29,0931) have been identified, but there are also peaks that cannot be assigned to known phases.

Finally, the time hold and ammonia flow do not seem to play a key role in the synthesis of these compounds. In practice, the nitrides can be prepared with 2 h of thermal treatment under different ammonia flows (see Table 1).

Chemical characterization

As indicated above, the results of the metal analyses in all the nitride samples give (within experimental error) a molar ratio total-M to Mo content equal to unity (Table 3). In addition, dealing with the Fe and Co derivatives, the nitrogen content is consistent with M_3Mo_3N stoichiometry.

However, we have pointed out above that the ammonolysis of the nickel molybdate leads always to a mixture of the majority phase and minority impurities. Indeed, we have carefully studied the 1073 K 'nitride' samples [Fig. 3(b)] by EDAX to detect possible inhomogeneities in metal composition. The determination of the Ni : Mo ratio in different zones using small areas of irradiation gives unambiguously a Ni : Mo = 2 : 3 ratio for the majority phase, whereas an enrichment in Ni, as reflected by Ni : Mo ratios higher than 1 : 1, is observed in some definite zones. Thus, in spite of our inability to identify the nature of the impurities, the nitrogen content in the samples (Table 3) is consistent with the Ni_2Mo_3N composition for the majority phase.

Structure refinements of Fe_3Mo_3N and Co_3Mo_3N

The X-ray powder diffraction patterns of these compounds were indexed to primitive cubic unit cells, with cell parameters $a = 11.0752(4)$ Å (Fe_3Mo_3N) and 11.0188(5) Å (Co_3Mo_3N) from 13 accurately measured reflection positions using the TREOR program [figures of merit: $M_{13} = 57$, $F_{13} = 30$ (0.0053, 82) and $M_{13} = 44$, $F_{13} = 20$ (0.0077, 81), respectively]. Systematic absences were consistent with space groups $Fd\bar{3}$ and $Fd\bar{3}m$. These results indicate cells that should be similar to those proposed by Bem *et al.*[9,10] The structures have been refined in space group $Fd\bar{3}m$, using as a starting structural model that proposed for Fe_3Mo_3N.[10] Fig. 4 shows the observed and calculated patterns. Refined structural parameters and residuals, R_p, R_{wp}, R_B and R_F are listed in Table 4. A selected list of bond distances is summarized in Table 6. It must be stressed that, for a better estimation of the accuracy of the parameters, the standard deviations (that relate only to the precision of parameters), must be multiplied by the SCOR parameter, according to ref. 17. SCOR parameters have values of 1.96 and 1.88 for Fe and Co compounds.

Structure refinement of Ni_2Mo_3N

We have commented above that the Ni compound is obtained together with impurities under all the synthetic conditions explored in this work. In fact, the observation of impurities of different natures depending on the synthetic procedure can allow us to identify the peaks of the Ni majority phase. Taking into account only these peaks (that is to say, those peaks systematically appearing in the patterns from different preparations at fixed 2θ values and showing constant intensity ratios), the X-ray powder diffraction pattern of the Ni compound was indexed from 14 accurately measured, unambiguous reflection positions. A primitive cubic cell was obtained with a cell parameter $a = 6.6311(3)$ Å [figures of merit: $M_{14} = 139$ and $F_{13} = 79$ (0.0085, 21)]. Systematic absences were consistent with space groups $P4_132$, $P4_232$ and $P4_332$. A search in the inorganic crystal structure database shows that the isostructural compounds V_3Zn_2N, V_3Ga_2N and Nb_3Al_2N have similar cell parameters and systematic absences. However, the calculation of bond distances and angles from the proposed structural model gives unusually short metal–metal distances (< 1 Å) in all cases, indicating very likely some error in the proposed structural model. Then, in order to solve the structure, structure

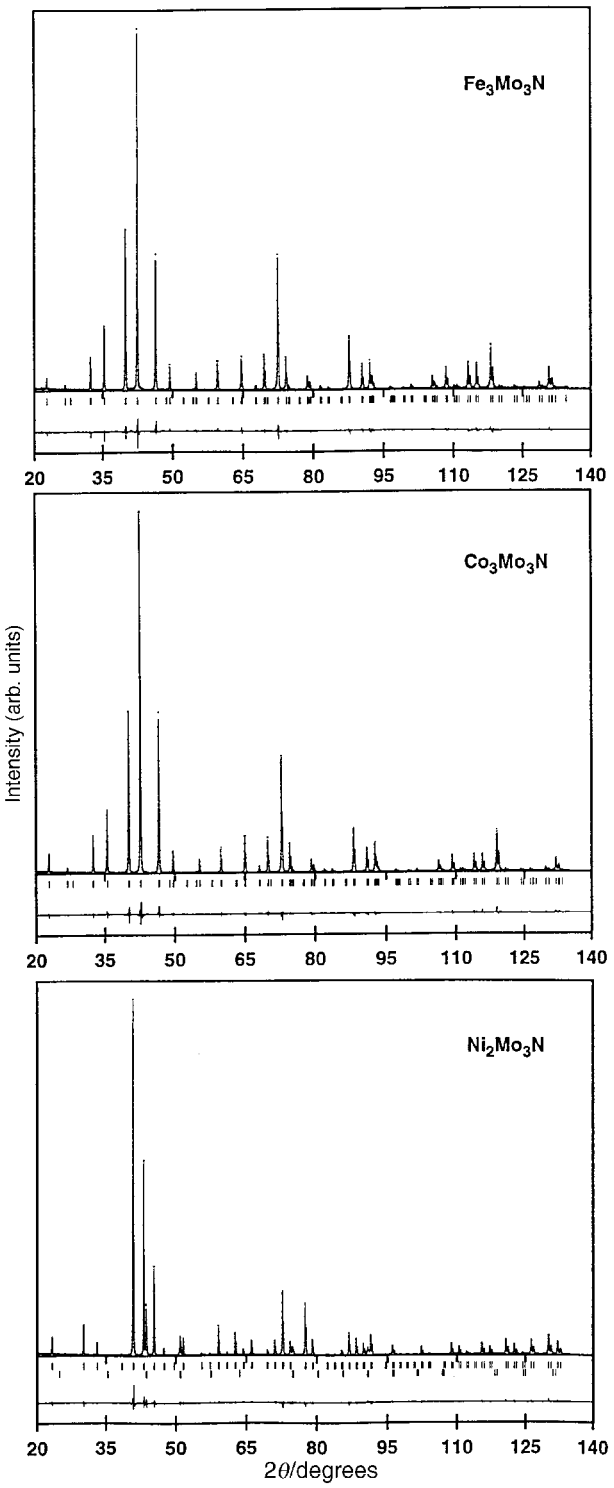

Fig. 4 Observed (dotted) and calculated (solid) X-ray diffraction profiles for Fe_3Mo_3N, Co_3Mo_3N and Ni_2Mo_3N. Tic marks below the diffractograms represent the allowed Bragg reflections. The residual lines are located at the bottom of the figures.

factors were extracted by profile fitting of the pattern (as result from the synthesis at 1223 K, fast cooling rate), using the Le Bail's method[18] as implemented in the FULLPROF program.[16] Reliable structural models were obtained by direct methods using the routines implemented in the SIRPOW program[19] for space groups $P4_132$ and $P4_332$. These solutions correspond to enantiomorphs. The starting structural model used for the refinement of the structure, performed using the FULLPROF program, was that obtained for space group $P4_132$. Both in the extraction of the structure factors and in the structural refinement, the impurity was treated as cubic, with a cell

Table 6 Selected bond distances (Å) for M_3Mo_3N (M = Fe, Co)

	Fe	Co
Mo—M(1) ×2	2.6623(9)[a]	2.6298(10)[a]
Mo—M(1) ×2	2.7706(11)[b]	2.7288(11)[b]
Mo—M(2) ×2	2.7819(5)[c]	2.7491(5)[c]
Mo—Mo ×4	2.8927(2)	2.8679(2)
Mo—Mo ×4	3.0794(7)	3.1042(7)
Mo—N ×2	2.1125(4)	2.1131(4)
M(1)—M(1) ×3	2.5433(13)	2.5830(12)
M(1)—M(2) ×3	2.3846(9)[d]	2.3836(9)[d]

M(1) coordination sphere is completed by 3 Mo at distances labelled *a*, and 3 Mo at distances labelled *b*; M(2) coordination sphere is defined by 6 Mo at distances *c*, and 6 M(1) at distances *d*.

Table 7 Selected bond distances (in Å) for Ni_2Mo_3N

Ni—Ni ×3	2.4708(16)
Ni—Mo ×3	2.7341(12)
Ni—Mo ×3	2.7372(12)
Ni—Mo ×3	2.8162(12)
Mo—Mo ×4	2.7745(7)
Mo—Mo ×2	2.8206(7)
N—Mo ×6	2.0818(4)

parameter of 3.590 Å (see above), and their intensities adjusted using the pattern matching option of the FULLPROF program. It must be stressed that there is no overlapping between the impurity peaks and the peaks proper of the phase. In the structural refinement, the individual site occupancies are allowed to vary, and the structure converged with nickel atoms in the 8c site, and a 98.6(8)% occupation of the 12d sites by molybdenum atoms [1.4(8)% of nickel atoms], which is consistent with the stoichiometry determined by EDAX for this phase. Thus, within the experimental error, the stoichiometry obtained from the Rietveld refinement is Ni_2Mo_3N. Fig. 4 shows the observed and calculated patterns. Refined structural parameters and residuals, R_p, R_{wp}, R_B and R_F are listed in Table 5. A selected list of bond distances is summarized in Table 7. The SCOR parameter value is 1.87.

Description of the structures

The structure of M_3Mo_3N (M = Fe, Co) consists of a distorted fcc arrangement of the metallic atoms (M and Mo), with N atoms occupying distorted octahedral interstitial sites. Each Mo atom is surrounded by four Mo, six M and two N atoms, to give $Mo[Mo_4M_6N_2]$ entities. The distances from the 'central' Mo atom to the remaining metallic atoms in these entities range from *ca.* 2.63 to *ca.* 2.89 Å. In addition, there are another four Mo atoms at somewhat larger distances, *ca.* 3.10 Å. There are two different structural sites for M atoms. In each, M atoms are surrounded by six Mo and six M atoms, to give $M[Mo_6M_6]$ units. Finally, each N atom is surrounded by six Mo atoms, defining a distorted octahedron $[NMo_6]$. These octahedra share faces.

The structure of Ni_2Mo_3N consists of a β-Mn arrangement of metallic atoms (Ni and Mo), with N atoms occupying distorted octahedral interstitial sites. As is well known, in the β-Mn structure there are two different types of metallic atom sites, which have different multiplicities (Wyckoff positions 8c and 12d in space group $P4_132$). Ni_2Mo_3N turns out to be a nice example of coloring[20] of this structural type: Ni atoms occupy the 8c sites and Mo atoms the 12d sites. The result is that each Ni atom is surrounded by three Ni and nine Mo atoms, giving $Ni[Ni_3Mo_9]$ units. In turn, each Mo atom is surrounded by six Ni, six Mo and two N atoms, giving $Mo[Ni_6Mo_6N_2]$ entities. Finally, each N atom is surrounded by six Mo atoms, defining a distorted octahedron. These $[NMo_6]$ octahedra share corners.

In a general way, molybdenum ternary nitrides can be classified into two groups: ionic/covalent and interstitial nitrides. Ionic/covalent nitrides are characterized by metal to nitrogen ratios close to unity. In turn, these nitrides can be defined as ionic (as in Na_3MoN_3 or Ba_3MoN_4[21,22]), having short Mo—N bond distances [1.88(1) and 1.92(1) Å, respectively], and covalent [$MnMoN_2$,[8] $LiMoN_2$,[23] $(Fe_{0.8}Mo_{0.2})MoN_2$[9]], with large Mo to N bond distances [2.120(2), 2.095(4)/2.091(4) and 2.130(3) Å, respectively]. In contrast, the M_nMo_3N derivatives studied in this work are clearly interstitial nitrides, from the structural point of view, as expected from their high total-metal to nitrogen stoichiometric ratios (6:1 for M = Fe, Co; 5:1 for M = Ni). The Mo to N bond distances found in this work are similar to those reported for covalent nitrides. This fact, besides the selective occupation by the N atoms of interstices defined only by Mo atoms, suggests a covalent character of the Mo—N bonding in these M_nMo_3N interstitial compounds. On the other hand, concerning the metal–metal distances, the experimental Mo—M ones are similar to those found in covalent molybdenum nitrides. However, the M—M bond distances are significantly shorter than those found in other transition metal molybdenum or tungsten ternary nitrides [Fe—Fe 2.876 30(5) and 2.8562(1) Å for $FeWN_2$[8] and $(Fe_{0.8}Mo_{0.2})MoN_2$,[9] and Mn—Mn distances of 2.922 62(8) Å in $MnMoN_2$[8]].

Microstructural characterization

The morphology of the precursors and ternary nitrides (Fig. 5) was observed using scanning electron microscopy (field emission). SEM scanning images show that the precursors are formed by elongated crystals with typical dimensions around $1500 \times 150 \times 150$ nm for Fe and Co precursors, and $800 \times 100 \times 100$ nm for the Ni precursor. In all cases, the thermal treatment induces significant changes in the microstructure compared with the initial precursors, affecting both the particle size and morphology (from very elongated prisms to rounded particles) [Fig. 5(a) and (b)]. These changes clearly indicate that the transformation during nitridation is not pseudomorphic, in contrast to that observed in the nitridation of vanadium oxide.[24] Besides this, a progressive increase with temperature is observed in the particle size in the Fe and Co cases [samples prepared at 973 K have mean particle sizes below 250 and 125 nm, whereas at 1173 K these are around 1000 and 500 nm, respectively, Fig. 5(c) and (d)]. Similarly, a progressive increase in particle size with the reaction time was observed for the Ni and Co compounds [from 500 nm for 2 h to 1000 nm for 12 h at 1073 K, in the case of the Ni compound, Fig. 5(e) and (f)].

Oxidation behavior

Fig. 6 shows characteristic TPO profiles and TGA curves for all three nitrides.

For Fe_3Mo_3N, oxidation begins at *ca.* 450 K. Two peaks are observed in the TPO profile at 593 and 744 K, associated with two discontinuities in the TGA curve. The X-ray diffraction pattern of a sample oxidized at 650 K shows the presence of two phases, Fe_3Mo_3N (majority phase) and β-$FeMoO_4$ (minority phase; JCPDS card 22,0628). The oxidation is complete at 850 K, the oxidation product being a mixture of $Fe_2(MoO_4)_3$ (JCPDS card 31,0642 and 35,0183) and Fe_2O_3 (JCPDS card 36,0526). At temperatures above 1000 K, the TGA curve shows a weight loss (not shown in Fig. 6) that can be attributed to the decomposition of iron(III) molybdate and subsequent sublimation of MoO_3.

The oxidation of Co_3Mo_3N and Ni_2Mo_3N follows a similar course. It begins at *ca.* 500 K and is complete at *ca.* 1000 K in both cases. However, several TPO peaks (associated with effects in the TGA curves) are observed prior to the maximum oxygen consumption, which occurs at 830 and 882 K for the Co and Ni samples, respectively. The final oxidation products

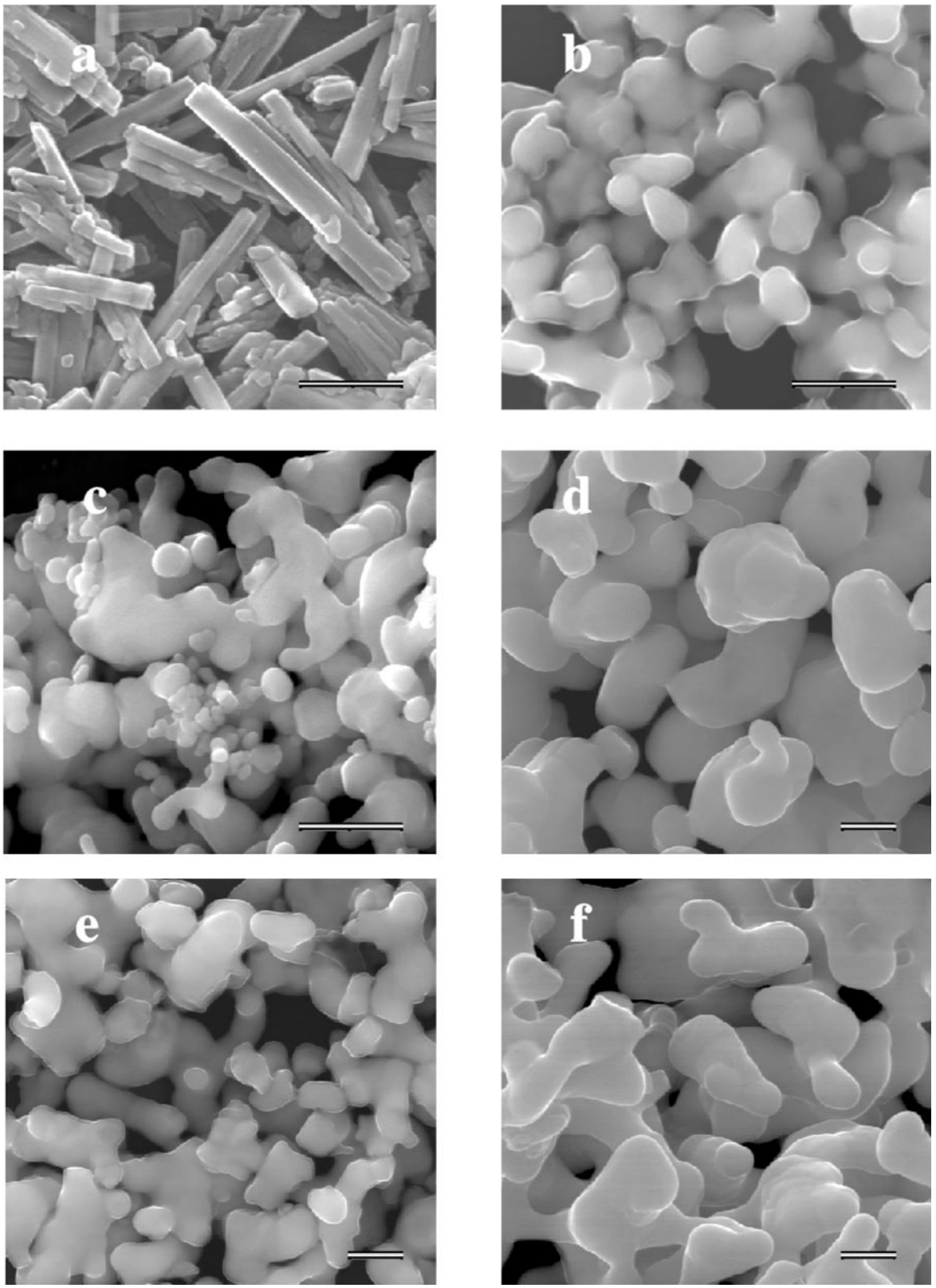

Fig. 5 SEM images showing the microstructure of: (a) as-dried CoMoO precursor; (b) Co_3Mo_3N nitride prepared at $T_f = 1173$ K, $t_h = 2$ h (sample CoMoN-F); (c) Fe_3Mo_3N nitride prepared at $T_f = 1073$ K, $t_h = 12$ h (sample FeMoN-C); (d) Fe_3Mo_3N nitride prepared at $T_f = 1173$ K, $t_h = 12$ h (sample FeMoN-F); (e) Ni_2Mo_3N nitride prepared at $T_f = 1073$ K, $t_h = 2$ h (sample NiMoN-D) and (f) Ni_2Mo_3N nitride prepared at $T_f = 1073$ K, $t_h = 12$ h (sample NiMoN-C). Scale bars correspond to 500 nm.

are identified as $CoMoO_4$ (JCPDS card 21,0868 and 25,1434) and $NiMoO_4$ (JCPDS card 33,0948). The X-ray diffraction pattern of the Co sample oxidized up to 700 K shows the presence of a mixture of Co_3Mo_3N (majority phase), $CoMoO_4$ and $CoMoO_3$ (minority phases; JCPDS card 22,0628 and 21,0868, respectively). For the Ni sample oxidized at 750 K, a mixture of Ni_2Mo_3N, a phase with a pattern very similar to $Ni_{0.2}Mo_{0.8}N$ (JCPDS card 29,0931) and a cubic impurity are identified.

These results indicate that Fe_3Mo_3N is the least stable among the three ternary molybdenum nitrides under study with respect to oxidation. On the other hand, the non-

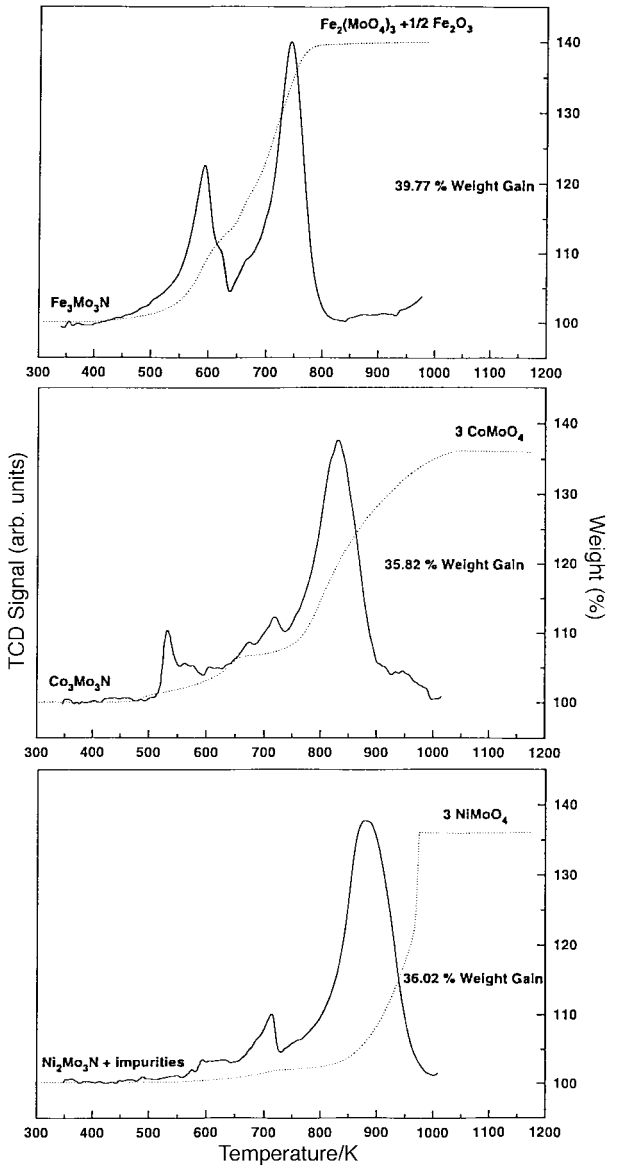

Fig. 6 TPO (continuous lines) and TGA (broken lines) profiles corresponding to transition metal nitrides: Fe_3Mo_3N (sample FeMoN-C), Co_3Mo_3N (sample CoMoN-C) and Ni_2Mo_3N (sample NiMoN-C)

observation of intermediate phases (oxynitrides) for the oxidation of Fe_3Mo_3N and Co_3Mo_3N, together with the pyrophoric character of some of the products, suggests that the low temperature oxidation steps correspond to superficial oxidation phenomena. In fact, the X-ray diffraction patterns of the pyrophoric products are similar to those obtained at intermediate temperatures for the oxidation processes. For the nickel compound, however, low temperature oxidation does not lead to nickel molybdate (so discarding a superficial oxidation of Ni_2Mo_3N as the origin of this step), thus indicating that the nickel–molybdenum nitride is more stable in an oxygen atmosphere. The low temperature oxidation step is probably associated to oxidation of impurities.

On the other hand, in all three cases the total mass gains are slightly smaller than the theoretical values corresponding to the oxidation of the nitride to the respective metal molybdate (and Fe_2O_3, for Fe_3Mo_3N). This suggests the presence of some oxygen in the samples and, in fact, it was detected by EDAX (although, as expected, it was not possible to quantify). The experimental mass gains are consistent with the presence of 1–2% of oxygen in the samples, values that are similar to that reported in the characterization of $(Fe_{0.8}Mo_{0.2})MoN_2$.[9] Taking into account the oxidation behavior, as well as the pyrophoric

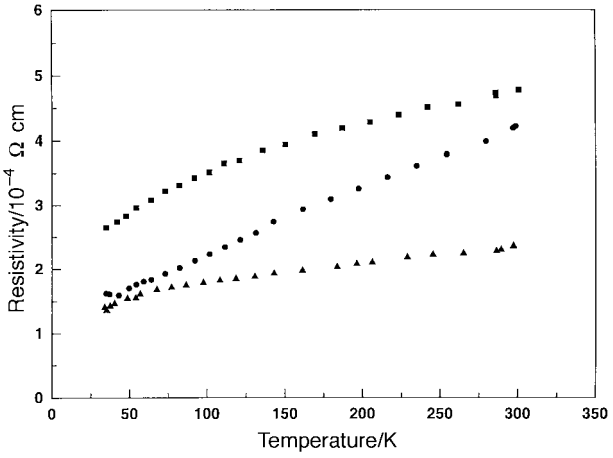

Fig. 7 Temperature dependence of the resitivity for sintered pellets of Fe_3Mo_3N (■), Co_3Mo_3N (▲) and Ni_2Mo_3N (●) materials

character of some of the samples, it seems reasonable to assign this deviation to superficial oxidation of the nitrides (undetectable by X-ray diffraction).

Electric measurements

Dc resistivity measurements (Fig. 7) show that all three M_nMo_3N interstitial nitrides exhibit metallic behavior, which is practically temperature independent. In spite of the fact that the measurements have been performed on pressed pellets, including thus grain boundary resistance contributions, which may significantly decrease the conductivity, dc resistivity values are approximately four orders of magnitude lower than those reported for ternary molybdenum ionic/covalent nitrides,[9] as would be expected from their structural features.

Concluding remarks

From the available information, molybdenum-containing bimetallic nitrides constitute complex systems that may include various definite phases of different chemical natures. In this context, nitrogen-poor interstitial nitrides should relatively be entropy favoured materials, which have to be processed within a given high temperature range. To delimit both the appropriate conditions to optimize the yield in each possible phase and to achieve preparative procedures as mild as possible, are crucial for further applications. As opposed to the traditional 'heat and beat' procedure, those based on the use of bimetallic oxides as precursors intend to lend advantage from the expected decrease of the diffusion distances of the metallic atoms.

We have shown in this work both the usefulness of such a procedure (for Fe and Co derivatives) and some of its inherent limitations, as found in the Ni—Mo—N system. As far as the stoichiometric ratio of the metals in the resulting product (considered as a whole) is the same as that initially present in the precursor, the presence of impurities together with the main phase will usually occur when the proportion of the metal in the nitride differs from that of the starting oxide (a fact that, in some way, is likely to be the basis of erroneous results previously reported in the literature concerning the 'Ni_3Mo_3N' nitride[11,12]). Thus, the utility of this procedure when dealing with some well established compositions, appears of use in designing alternative synthetic procedures in order to explore different metallic compositions in complex systems such as those we are dealing with. The use of polymetallic precursors resulting from freeze-drying of aqueous solutions has proven to be a powerful technique in overcoming the problem of stoichiometry in the case of complex oxides, such as in high T_c superconducting materials,[25] although we must

bear in mind the significant differences in the chemical activity of the components of the involved systems. In fact, preliminary results relating to the preparation by this method of pure Ni_2Mo_3N has been satisfactory.[26] In contrast, even though the results obtained from ammonolysis of cobalt molybdate suggest the existence of a cobalt ternary nitride phase isostructural to Ni_2Mo_3N, we have been not able, as yet, to isolate it, and further study is in progress.

This research was supported by the Spanish Comision Interministerial de Ciencia y Tecnología (MAT96-1037). The SCSIE of the Universitat de València is acknowledged for X-ray diffraction and analytical facilities. S. A. acknowledges the Fondo para el Mejoramiento de la Calidad Universitaria (FOMEC) and the Universidad del Litoral for a grant for her stay in Spain.

References

1 (*a*) *The Chemistry of Transition Metal Carbides and Nitrides*, ed. S. T. Oyama, Blackie Academic & Professional, Chapman & Hall, London, 1996, p. 1; (*b*) *International Symposium on Nitrides*, in *J. Eur. Ceram. Soc*., ed. Y. Laurent and P. Verdier, 1997, vol. 17, p. 1773–2037.
2 A. T. Santhanam, in *The Chemistry of Transition Metal Carbides and Nitrides*, ed. S. T. Oyama, Blackie Academic & Professional, Chapman & Hall, London, 1996, p. 28.
3 K. Machida and G. Adachi, in *The Chemistry of Transition Metal Carbides and Nitrides*, ed. S. T. Oyama, Blackie Academic & Professional, Chapman & Hall, London, 1996, p. 191.
4 (*a*) S. Yamanaka, H. Kawaji, K. Hotehama and M. Ohashi, *Adv. Mater*., 1996, **8**, 771; (*b*) H. Kawaji, K. Hotehama and S. Yamanaka, *Chem. Mater*., 1997, **9**, 2127.
5 *Catal. Today*, 1992, **15**, High surface area nitrides and carbides, ed. P. W. Lednor.
6 (*a*) J. C. Schlatter, S. T. Oyama, J. E. Metcalfe and J. M. Lambert, *Ind. Eng. Chem. Res*., 1988, **27**, 1648; (*b*) C. H. Jaggers, J. N. Michaels and A. M. Stacy, *Chem. Mater*., 1990, **2**, 150; (*c*) C. W. Colling, J. G. Choi and L. T. Thompson, *J. Catal*., 1996, **160**, 35 and references therein.
7 (*a*) C. C. Yu, S. Ramanathan, F. Sherif and S. T. Oyama, *J. Phys. Chem*., 1994, **98**, 13 038; (*b*) C. C. Yu and S. T. Oyama, *J. Solid State Chem*., 1995, **116**, 207; (*c*) C. C. Yu and S. T. Oyama, *J. Mater. Sci*., 1995, **30**, 4037; (*d*) R. Kapoor, S. T. Oyama, B. Frühberger and J. G. Chen, *J. Phys. Chem. B*,1997, **101**, 1543.
8 D. S. Bem, C. M. Lampe-Onnerud, H. P. Olsen and H.-C. zur Loye, *Inorg. Chem*., 1996, **35**, 581.
9 D. S. Bem, H. P. Olsen and H.-C. zur Loye, *Chem. Mater*., 1995, **7**, 1824.
10 J. D. Houmes, D. S. Bem and H.-C. zur Loye, *MRS Symposium Proceedings: Covalent Ceramics II: Non-Oxides*, ed. A. R. Barron, G. S. Fischman, M. A. Fury and A. F. Hepp, Materials Research Society, Boston, MA, 1993, vol. 327, p. 153.
11 D. S. Bem, C. P. Gibson and H.-C. zur Loye, *Chem. Mater*., 1993, **5**, 397.
12 K. S. Weil and P. N. Kumta, *Mater. Sci. Eng. B*, 1996, **38**, 109.
13 X. Z. Chen, J. L. Dye, H. A. Eick, S. H. Elder and K.-L Tsai, *Chem. Mater*., 1997, **9**, 1172.
14 P. M. de Wolf, *J.Appl. Crystallogr*., 1968, **1**, 108.
15 G. S. Smith and R. L. Synder, *J. Appl. Crystallogr*., 1979, **12**, 60.
16 J. Rodriguez-Carvajal, FULLPROF Program, personal communication.
17 (*a*) J. F. Berar and P. Lelann, *J. Appl. Crystallogr*., 1991, **24**, 1; (*b*) J. F. Berar, *Acc. Powder Diffraction II, NIST Special Publ.,* 1992, **846**, 63.
18 A. Le Bail, H. Duroy and J. L. Fourquet, *Mater. Res. Bull*., 1988, **23**, 447.
19 G. Casacarano, C. Giacovazzo and A. Guagliardi, *Acta Crystallaogr*., *Sect. A*, 1992, **48**, 859.
20 J. K. Burdett, S. Lee and T. J. McLarnan, *J. Am. Chem. Soc*., 1985, **107**, 3083.
21 D. Ostermann, U. Zachwieja and H. Jacobs, *J. Alloys Compd*., 1992, **190**, 137.
22 A. Gudat, P. Höhn, R. Kniep and A. Rabenau, *Z. Naturforsch*., *Teil B*, 1991, **46**, 566.
23 S. H. Elder, L. H. Doerrer, F. J. Disalvo, J. B. Parise, D. Guyomard and J. M. Tarascon, *Chem. Mater*., 1992, **4**, 928.
24 S. T. Oyama, R. Kapoor, H. T. Oyama, D. J. Hofmann and E. Matijevic, *J. Mater. Res*., 1993, **8**, 1450.
25 V. Primo, F. Sapiña, M. J. Sanchis, R. Ibañez, A. Beltrán and D. Beltrán, *Solid State Ionics*, 1993, **63–65**, 872.
26 S. Alconchel, F. Sapiña, A. Beltrán and D. Beltrán, in preparation.

Paper 8/01643G; *Received* 26*th February*, 1998